Student thesis series INES nr 614

Monitoring deforestation in the Serranía de Chiribiquete in northern Colombian Amazon using time series analysis of satellite data

Yuyang Qian

2023
Department of
Physical Geography and Ecosystem Science
Lund University
Sölvegatan 12
S-223 62 Lund
Sweden

Yuyang Qian (2023).

Monitoring deforestation in the Serranía de Chiribiquete in northern Colombian Amazon using time series analysis of satellite data

Master degree thesis, 30 credits in *Geomatics*

Department of Physical Geography and Ecosystem Science, Lund University

Level: Master of Science (MSc)

Course duration: *January* 2023 until *June* 2023

Monitoring deforestation in the Serranía de Chiribiquete in northern Colombian Amazon using time series analysis of satellite data

---

Yuyang Qian

Master thesis, 30 credits, in *Geomatics*

Supervisor:

Jesica M. López
Centre for Environmental and Climate Science, Lund University
Lars Eklundh
Dep. of Physical Geography and Ecosystem Science, Lund University

Exam committee:

Abdulhakim M. Abdi
Centre for Environmental and Climate Science, Lund University

Acknowledgments

During the process of completing my thesis report, I received a lot of support and help. First of all, I would like to express my gratitude to my supervisor, Jesica López, who provided valuable opinions from topic selection to writing the thesis. She is very approachable and kind. She always encourages me whenever I complete a part of the task, urging me to do better. Whenever I have questions, she always tries her best to answer them until I fully understand. At the same time, Jesica also cares a lot about my future development and has provided a lot of help with my PhD application.

Second, I am very grateful for the revision suggestions made by Lars and Hakim on my thesis. Although some feedback was harsh, it was valuable and useful which made me find the shortcomings of my thesis.

Third, I would like to thank Jamali and Paulo for providing the inspiration for the method and technical guidance.

Finally, I would also like to thank my parents for their support on both material and spiritual levels throughout my two years of study. They always support my choices and are my strong backing. I would like to thank Liverpool Football Club for accompanying me during the weekend, which has helped me understand that winning and losing are only temporary moments in life and you'll never walk alone.

Abstract

Deforestation monitoring is of significant importance for the ecosystem, climate change, and policy-making. The availability of optical and synthetic aperture radar (SAR) satellite remote sensing images, along with the development of time series change detection methods, has contributed to the increasing popularity of time series analysis in forest disturbance monitoring. However, there are few studies that compare the performance of optical and SAR imagery for this purpose. In this study, the Landsat and Sentinel-1 time series imagery from 2016 to 2021 was used to detect forest cover loss in the northern Colombian Amazon, which has experienced great deforestation following the signing of the Colombian peace agreement in 2016. The time series change detection method applied in this study is the Continuous Change Detection and Classification (CCDC) algorithm, as it flags land cover changes by differencing the predicted and observed data. The deforestation detected by 1040 Landsat and 1378 Sentinel-1 images indicates that deforestation gradually increased from 2016 to 2018 and then exhibited a fluctuating trend. The peak years of deforestation were observed in 2018 and 2020. The paired-samples t-test revealed that the difference between detected forest loss area by Landsat and Sentinel-1 data is statistically significant in study region 1, while it is not statistically significant in study region 2. Furthermore, the spatial distribution analysis indicated that the detected forest loss from 2016 to 2021 roughly followed the direction of the boundaries of the protected area. After assessing the accuracy using stratified random sampling, the overall accuracy values of 62.7% for Landsat and 43.3% for Sentinel-1 in detecting deforestation were obtained. Subsequently, a temporal accuracy assessment of the forest disturbance pixels successfully detected by Landsat and Sentinel-1 was conducted. The results showed that 62.8% of Landsat pixels and 74.9% of Sentinel-1 pixels accurately matched the corresponding actual years of deforestation. This study suggests that integrating Landsat and Sentinel-1 data for forest disturbance monitoring may potentially yield better results in both spatial and temporal domains.

Keywords: CCDC, Forest loss, Landsat, Sentinel-1, Change detection, NNP, FARC

Contents

1 Introduction

Forests are key components of the ecological system all over the world. Among the different forest categories, tropical forests are difficult to regenerate after wildfires, they are rich in biodiversity, and store approximately 470 billion tons of carbon which is far more than what is stored in temperate and boreal forests (Seymour and Busch, 2016). Deforestation, which is the conversion from forests to other land cover types, has a significant effect on environmental and social aspects in these ecosystems (Arias-Gaviria et al., 2021). From 2001 to 2019, forest disturbances, including deforestation, contributed to global gross greenhouse gas emissions of 8.1±2.5 Gt CO2e yr^{-1}, and 78% of emissions came from tropical and subtropical forests (Harris et al., 2021).

Colombia is a country that is strongly affected by loss of tropical forest. The rate of deforestation in the Protected Areas of Colombia and its buffer areas has increased since the Colombian government and the Revolutionary Armed Forces of Colombian (FARC) signed the peace agreement in 2016. According to the official data, due to complicated socio-economic dynamics such as agriculture, illicit crops and cattle ranching, as well as the construction of human settlements and roads, approximately 340,000 hectares of land in Colombia are at risk of deforestation by 2024 (Clerici et al., 2020). The extensive cattle ranching activities are a major land use in the Amazonian region of Colombia and the main driver of forest conversion (Murillo-Sandoval et al., 2022). The increase of cattle ranching in the Colombian Amazon has resulted in significant deforestation in eight municipalities around the National Natural Park Serranía de Chiribiquete in the northwestern part of the region.

As remote sensing technology continues to advance, satellite data is becoming increasingly recognized as a valuable tool for monitoring forest change, and researchers are focusing more attention on its potential (Zhong et al., 2020). Among these data, optical satellite data is commonly used to monitor tree cover losses which can be generally divided into two categories: regional and global scale data. For example, low

spatial resolution remote sensing data such as MODerate resolution Imaging Spectroradiometer (MODIS) and Advanced Very High Resolution Radiometer (AVHRR) data are frequently employed for monitoring forest change over large areas. Previous studies have demonstrated that the use of MODIS and AVHRR data allows for quick identification of deforestation areas and at the same time reducing storage and processing requirements (Di Maio Mantovani and Setzer, 1997; Morton et al., 2005).

Compared to coarse spatial resolution data, Landsat imagery has higher spatial resolution and is often used by researchers for regional-scale forest disturbance monitoring (Hansen and Loveland, 2012). Landsat offers the longest historical archive dataset of earth observation at moderate spatial resolution (30 m), and it is freely available. Therefore, current research for regional-scale monitoring of forest change using medium spatial resolution imagery commonly relies on Landsat data (Hansen and Loveland, 2012).

In addition to the mentioned low and medium spatial resolution satellites, high spatial resolution satellites can also be used to monitor deforestation. For instance, PlanetScope satellites provide an exceptional blend of 3 m spatial resolution and daily temporal resolution. This is beneficial to detect forest cover loss at sub-annual scales (Francini et al., 2020). Nevertheless, most high spatial resolution satellites are owned by commercial companies and not freely distributed. Additionally, utilizing high spatial resolution images for monitoring deforestation in large study areas can be time-consuming.

Nowadays, using optical satellite data to detect deforestation is popular and has achieved remarkable success. However, some inaccurate information may occur due to cloud cover in tropical forests, especially in rainy seasons. As an alternative, Synthetic Aperture Radar (SAR) data can also be used to monitor deforestation because it is independent of weather conditions compared with optical satellite data (Reiche et al.,

2018; Reiche et al., 2021). In the past, only a few studies used SAR data for monitoring deforestation due to a lack of sufficient SAR data (Pasquarella et al., 2022). A new era in SAR monitoring began with the launch of the Sentinel 1A and 1B satellites in April 2014 and April 2016, respectively. These two satellites supply a vast amount of free data for the Copernicus program's operational requirements (Bouvet et al., 2018). Lohberger et al. (2018) were among the first researchers to publish a paper using Sentinel-1 for detecting forest disturbances caused by forest fire. Additionally, Reiche et al. (2018) developed innovative techniques that combine various satellites, including Sentinel-1, PALSAR-2, and Landsat, for detecting forest disturbances.

Many studies have based forest change detection on comparing pairs of classified images, which is time-consuming and inefficient. Furthermore, this method is not accurate enough for long-term analysis and cannot meet the demands of practical applications (Zhong et al., 2020). Besides, during the process of change detection, seasonal changes caused by variations in solar angle and vegetation phenology are often considered the primary sources of noise in change detection (Zhong et al., 2020). To avoid these issues, researchers typically select images taken during the same season or correct for these seasonal changes using de-seasoning methods (Zhu, 2017). The ability of time series analysis to replace the bitemporal image comparisons approach is contingent upon the availability of preprocessed long-term satellite remote sensing data, as well as the continued enhancement of automated algorithms capable of extracting information that characterizes various forest dynamics, including forest cover loss (Banskota et al., 2014).

During recent years, Google Earth Engine (GEE) has become a strong tool for rapid remote sensing cloud computing on account of its vast data resources and strong computational capabilities. GEE stores commonly used satellite remote sensing data including Landsat and Sentinel (Brovelli et al., 2020). Moreover, time series change detection methods such as Landsat-based detection of Trends in Disturbance and

Recovery (LandTrendr) and Continuous Change Detection and Classification (CCDC) are implemented in GEE. For example, the LandTrendr algorithm relies on the Normalized Burn Ratio (NBR) as its primary indicator of change and assumes the time series data already exist (Zhu, 2017). The CCDC algorithm utilizes all spectral bands of all available Landsat data and assumes the time series data is being received at a specific interval (Zhu, 2017). Both LandTrendr and CCDC have been successfully applied to analyze forest change detection and land cover change detection (Pasquarella et al., 2022). Leveraging the advantages of cloud computing using GEE, the processing speed of LandTrendr and CCDC algorithms has significantly increased. This has provided a massive opportunity for large-scale implementation of these algorithms in identifying forest change in regions of interest (Pasquarella et al., 2022).

In studies aiming to detect deforestation based on LandTrendr and CCDC algorithms, optical satellite data is used, and few studies have utilized SAR data. Bullock et al. (2022) applied SAR data only to the CCDC algorithm for the first time, showing that CCDC and Sentinel-1 monitoring system can detect change events. However, in most cases, SAR data is used in combination with optical data (Fu et al., 2022; Shimizu et al., 2019). Although data fusion can provide more accurate results (Shimizu et al., 2019), it is necessary to evaluate the performance of individual use of optical or SAR data when detecting deforestation (Joshi et al., 2016). To date, there is no research focusing on this topic currently in the identification of forest cover loss in the Colombian Amazon. Considering the lack of literature on the application of SAR data to the Landtrendr algorithm, as well as the fact that the algorithm's input is based on a yearly time series, this study chose the CCDC algorithm as the methodological approach to detect deforestation (Pasquarella et al., 2022).

The overall aim of this project is to compare the performance of Landsat and Sentinel-1 data on the monitoring of deforestation in the northern Colombian Amazon between 2016 and 2021 by using the CCDC algorithm. This will be achieved through the

following research objectives:

(1) To investigate the area of deforestation in the northern Colombian Amazon between 2016 and 2021;

(2) To compare Landsat and Sentinel-1 accuracies under the CCDC algorithm for change detection.

2 Background

2.1 Remote sensing data for monitoring deforestation

Currently, multispectral and SAR data are the most widely used data sources to monitor deforestation. However, both have their own strengths and weaknesses based on imaging principle. The remote sensing data to choose for research purposes depends on the study area, study period and other factors. In terms of the study area, characteristics such as the size, land cover types, topography, and weather conditions, determine the requirements of the remote sensing data (Joshi et al., 2016). For example, if the study area is large, medium or coarse spatial resolution data may be useful because of less data storage. Besides, the study period also plays a crucial role in remote sensing data selection. If the study period is long (i.e., from 2000 to present), Landsat or MODIS data could be a viable choice due to their long historical archive. Moreover, data availability and budget constraints will also influence the data selection process. Landsat, Sentinel, and MODIS are popular choices for obtaining freely available satellite imagery due to their accessibility and affordability. However, higher resolution data, such as PlanetScope or Unmanned Aerial Vehicle (UAV) imagery, may be better for more detailed analysis, but is more expensive and difficult to acquire. The following section will describe the basic principles and commonly used satellites of optical imagery and SAR imagery, as well as their applications in deforestation detection.

2.1.1 Multispectral data

Electromagnetic radiation is a fundamental means of energy transportation. By detecting and measuring electromagnetic radiation using sensors implemented on

satellites or UAV, images in different wavelengths such as visible light (Blue, Red, Green), near-infrared (NIR), shortwave infrared (SWIR) and thermal infrared (TIR) can be captured. Table 1 introduces some commonly used multispectral satellites (Drusch et al., 2012; Wulder et al., 2022).

Table 1. Summary of technical characteristics of Landsat and Sentinel 2 satellites.

Satellites	*Spectral bands and spatial resolution*	*Temporal resolution*	*Lifetime*
Landsat 4	Blue, Red, Green, NIR, SWIR (30 m) TIR (120 m)	16 days	1982-1993
Landsat 5	Blue, Red, Green, NIR, SWIR (30 m) TIR (120 m)	16 days	1984-2013
Landsat 7	Blue, Red, Green, NIR, SWIR (30 m) TIR (60 m)	16 days	1999-2022
Landsat 8	Blue, Red, Green, NIR, SWIR, Coastal Aerosol, Cirrus (30 m) TIR (100 m)	16 days	2013-present
Sentinel 2	Blue, Red, Green, NIR (10 m) Vegetation Red Edge (20 m) Coastal Aerosol/Water Vapour/Cirrus (60 m) SWIR (20 m)	5 days	2015-present

Landsat is the most used satellite to detect deforestation because of its long historical archive. However, due to its 16-day revisit cycle and effect of cloud cover, Landsat is limited to detect changes in tropical forests. The fusion between Landsat and Sentinel 2 data supplies the possibility to increase the global average revisit interval which enables clear observations for deforestation monitoring in certain regions (Chen et al., 2021).

2.1.2 SAR data

Different from multispectral data, SAR data is difficult to interpret visually as the information on a SAR image is the response of the terrain features relative to the radar beam, mainly formed by the backscattering of the terrain features (Lichun, 2009). Different structures of terrain features and different wavelengths, polarizations of SAR sensors result in distinguishable textures and shades of SAR images (Lichun, 2009). In

Table 2 several SAR satellites are included (Tsokas et al., 2022).

Table 2. Summary of technical characteristics of SAR satellites.

Satellites	*Band*	*Wavelength*	*Polarization*	*Lifetime*
ALOS-1	L-band	24.6 cm	Single, Dual, Full (dependent)	2006-2011
ALOS-2; PALSAR-2	L-band	24.6 cm	Single, Dual, Full (dependent)	2014-present
Radarsat-1	C-band	5.6 cm	Horizontal-Horizontal (HH)	1995-2013
Radarsat-2	C-band	5.6 cm	Single, Dual, Full	2007-present
Sentinel-1	C-band	5.6 cm	Single, Dual (dependent)	2014-present

Compared with multispectral data, SAR data can be used under different weather conditions. Figure 1 shows the Landsat and Sentinel-1 images acquired on similar dates. From the figure, it is evident that the Landsat image quality is poorer due to the influence of clouds and cloud shadows, making it challenging to accurately identify ground features. In contrast, the Sentinel-1 image is not affected by these factors. With this advantage, C-band and L-band SAR data has proven their capability to detect deforestation, especially in tropical forests (Reiche et al., 2018). This is because SAR backscattering measurements from Vertical-Horizontal (VH) polarization and Vertical-Vertical (VV) polarization show an overall decrease following deforestation event (Doblas et al., 2020). However, a study illustrated that free and open-access L-band SAR data is less available, compared with C-band SAR data (Reiche et al., 2018). Even if users have access to L-band SAR data such as the ALOS-2 PALSAR-2 satellite data, only a few images per year are obtainable for most tropical regions which limits the application of monitoring deforestation (Reiche et al., 2018). On the contrary, with the help of Sentinel-1A and Sentinel-1B satellites, two widely used C-band SAR data sources, dense time series data with consistent acquisition properties can be acquired every 6 days for free (Schlund and Erasmi, 2020).

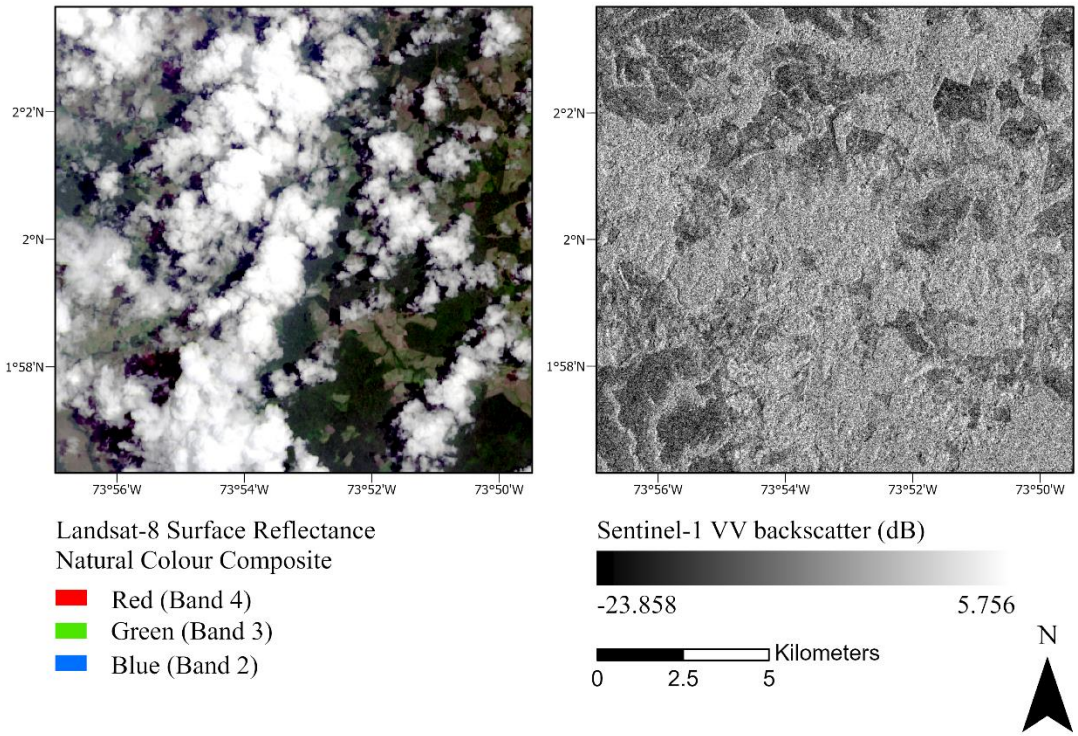

Figure 1. Landsat-8 image obtained from 10/09/2021 (left) and Sentinel-1 image obtained from 09/09/2021 (right) in the north of the Colombian Amazon.

2.2 CCDC time series change detection method

Time series change detection methods that are widely used today can be divided in two categories: i) online algorithms and ii) offline algorithms (Zhu, 2017). The online algorithms successively monitor changes as new data becomes available and the offline version operates on the entire time series to identify changes (Pasquarella et al., 2022). CCDC is an online algorithm which uses all available observation data in the time series to fit time series models. If new consecutive observations are beyond the expected range (3 times root mean square error), breakpoints are identified, and a new time series model is estimated, resulting in the generation of two time series segments: one before the breakpoint and one after it (Zhu and Woodcock, 2014).

The CCDC algorithm can identify all breakpoints in the specified time series and obtain information such as specific vegetation change time, which can be used in this study to detect forest cover changes. In addition to change detection, one of the advantages of CCDC is that it can perform land cover classification for any specific time during the

study period, which distinguishes it from other change detection methods (Zhu and Woodcock, 2014). Many studies have successfully applied the CCDC algorithm to land cover classification and change, near-real-time change detection, deforestation and forest degradation (Fu and Weng, 2016; Tang et al., 2019; Bullock et al., 2020). However, most research used optical satellites as data sources and there are few studies that applied the CCDC algorithm to SAR data, and this project will attempt to fulfill this knowledge gap in remote sensing science studies of deforestation in tropical ecosystems.

3 Study area and data sources

3.1 Study area

The Amazon region in Colombia has six departments, these are the Amazonas, Caquetá, Guainía, Vaupés, Guaviare, and Putumayo. In total, these departments cover 403,348 km^2 which are equivalent to approximately 5.4% of the total political-administrative Amazon basin, but they correspond to 35.3% of the continental Colombian territory (MADS, 2020). Between 2016 and 2018, the Colombian Amazon witnessed a surge in deforestation, which began after the signing of the FARC peace agreement in 2016. The deforestation rate peaked in 2018, with a historical high of 153,800 hectares. However, the estimated deforestation rate for 2019 has decreased significantly, returning to levels observed prior to the boom, at 53,800 hectares (Finer & Mamani, 2020).

The Picachos–Tinigua–Macarena–Chiribiquete corridor is a vital area within the Colombian Amazon as it facilitates the exchange of genetic material and dispersal of species (Clerici et al., 2019). In this region, habitat conversion, particularly deforestation caused by cattle ranching and illegal cultivation of coca, is a gradual and slow process that occurs frequently (Murillo-Sandoval et al., 2022). There are four main National Natural Parks (NNP) inside this corridor, including Tinigua, Sierra de la Macarena, Serranía de Chiribiquete and Cordillera de los Picachos (Clerici et al., 2019). This study focused on detecting deforestation in two regions from 2016 to 2021. The

study regions are close to northern and southern part of Serranía de Chiribiquete which is the largest NNP inside the corridor. Due to the increase of cattle ranching, these areas experienced severe deforestation. Figure 2 shows the two study regions with the background image from ArcGIS map service.

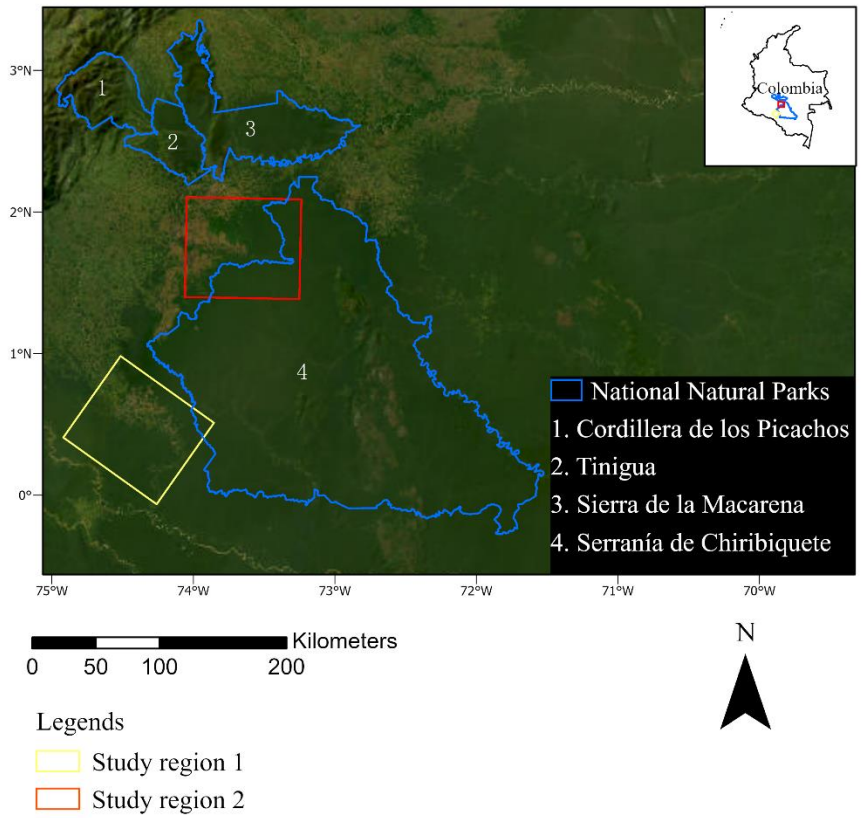

Figure 2. Study regions (focusing on north and south sections of the Serranía de Chiribiquete NNP).

3.2 Data sources

3.2.1 Sentinel-1 data

The Sentinel-1A/B SAR images used in this study were acquired from GEE. A total of 1378 available Sentinel-1 images in study regions between 2016 and 2021 were obtained for the analysis (Table 3). To prepare the dataset for analysis, multiple processing steps were undertaken. These steps included additional boundary noise correction, speckle filtering and radiometric slope correction (Mullissa et al., 2021). The border noise correction process removed regions at the edges of each image with

high or low incident angles (Stasolla and Neyt, 2018). Second, speckle noise was reduced based on multi-temporal speckle filtering by using Lee filtering with a kernel size of 9 (Quegan and Yu, 2001). The digital elevation model used for radiometric slope correction had a spatial resolution of 30 meters and was from the Shuttle Radar Topography Mission (Vollrath et al., 2020). The Radar Vegetation Index (RVI) which provides a quantitative measure of vegetation growth and density was calculated to fit CCDC time series models (Mandal et al., 2020). The RVI was calculated based on the VH and VV backscatter coefficient by using the following equation (Nasirzadehdizaji et al., 2019):

$$RVI = \frac{4VH}{VV + VH} \quad (1)$$

Another index applied to detect breakpoints refers to the Cross Ratio (CR) as it is sensitive to changes in the vegetation structure (Vreugdenhil et al., 2018). The CR was obtained by the ratio of VH and VV backscatter coefficient. After all the steps were completed, the SAR images were resampled to a resolution of 30 meters to reduce processing time and facilitate comparison with Landsat data.

Table 3. Total number of used Sentinel-1 images in study region 1 and 2.

	2016	*2017*	*2018*	*2019*	*2020*	*2021*
Region 1	25	140	138	188	205	190
Region 2	14	71	70	108	120	109
Total	39	211	208	296	325	299

3.2.2 Landsat data

All accessible Landsat 7 ETM+ and Landsat 8 OLI surface reflectance images (Collection 2, Tier 1) from 2016 to 2021 covering study areas were implemented in the study (Table 4). In total, there were 640 and 400 images in study region 1 and 2, respectively. Compared with Collection 1, Landsat Collection 2 data has improved geometric accuracy and radiometric calibration (Wulder et al., 2022). Landsat scenes that possess the highest quality are categorized as Tier 1 and are considered suitable for conducting time series analysis (Landsat Missions, n.d.). The spectral reflectance of ground objects in these datasets has been corrected for atmospheric effects using

sensors-specific algorithms, namely LEDAPS for ETM+ sensor (Masek et al., 2006) and LaSRC for OLI sensor (Vermote et al., 2016). Furthermore, to improve the quality of the data for the analysis, these datasets have been processed by CFMask algorithm to produce masks for clouds, shadows, and snow (Foga et al., 2017). It should be noted that this study did not fix the striping problem due to the Scan Line Corrector (SLC) error of Landsat 7. By using the tool developed by Arévalo et al. (2020), it is convenient and fast to get required Landsat data in GEE. This tool is established based on the GEE JavaScript API and includes a module to create Landsat stacks for the CCDC algorithm.

Table 4. Total number of used Landsat 7 and Landsat 8 images in study regions.

		2016	*2017*	*2018*	*2019*	*2020*	*2021*
Region 1	Landsat 7	43	56	58	50	54	53
	Landsat 8	55	59	52	55	47	58
	Total	98	115	110	105	101	111
Region 2	Landsat 7	30	29	28	35	34	43
	Landsat 8	37	36	33	34	30	31
	Total	67	65	61	69	64	74

3.2.3 PlanetScope data

Due to lack of in-situ information, the PlanetScope data was applied to evaluate the identified deforestation. The Global Forest Watch (GFW) map developed by Hansen et al. (2013) was not used as the reference data because it was created by Landsat data and failed to detect some deforestation areas compared to the PlanetScope data. To avoid bias and improve the reliability of the validation, PlanetScope imagery was chosen as the reference data. Norway's International Climate and Forest Initiative (NICFI) has recently released PlanetScope satellite images covering the tropical regions to preserve the tropical forests (Wagner et al., 2023). PlanetScope Visual Mosaics, one of data products provided by NICFI includes red, green and blue bands at a spatial resolution of about 5 meters for visual display and interpretation. These images have two types of temporal resolution which are bi-annual (from December 2015 to August 2020) and monthly (from September 2020 to present), respectively (NICFI, 2021). Since PlanetScope Visual Mosaics are composites of the best acquisitions, most images are

cloud free and clear. Therefore, these images are suitable for creating reference data in tropical regions. In addition to serving as reference data (Ygorra et al., 2021), high-resolution data from PlanetScope can also be directly used for detecting deforestation, significantly improving mapping of forest loss extent in tropical regions (Wagner et al., 2023).

3.2.4 FROM-GLC data

To better evaluate the effectiveness of the CCDC algorithm, a forest mask was generated to restrict detecting activities to forested regions (Figure 3). The purpose of creating the forest mask was to prevent potential confusion between changes happening in non-forest areas, such as crop harvest, and forest disturbances (Hamunyela et al., 2020). The forest mask is typically generated by classifying images that are close in time to the study period (DeVries et al., 2015; Guild et al., 2004). In this study, the land cover classification map in 2015, the closest available product to the start date of deforestation monitoring was downloaded and reclassified to generate the forest mask (Retrieved from: http://data.starcloud.pcl.ac.cn/zh/resource/3). This product is from the Finer Resolution Observation and Monitoring of Global Land Cover (FROM-GLC) project, providing the first 30 m spatial resolution global land cover maps based on Landsat data (Gong et al., 2013). The product categorizes land cover into 11 classes, including four subcategories within the forest class: mixed forest, broadleaf forest, needleleaf forest and orchard. The overall classification accuracy for all categories is approximately 64.9%. However, for the forest category, the overall accuracy of classification is greater than 70% (Gong et al., 2013). Further explanation of the use of the different data sources is explained in the methodology section below.

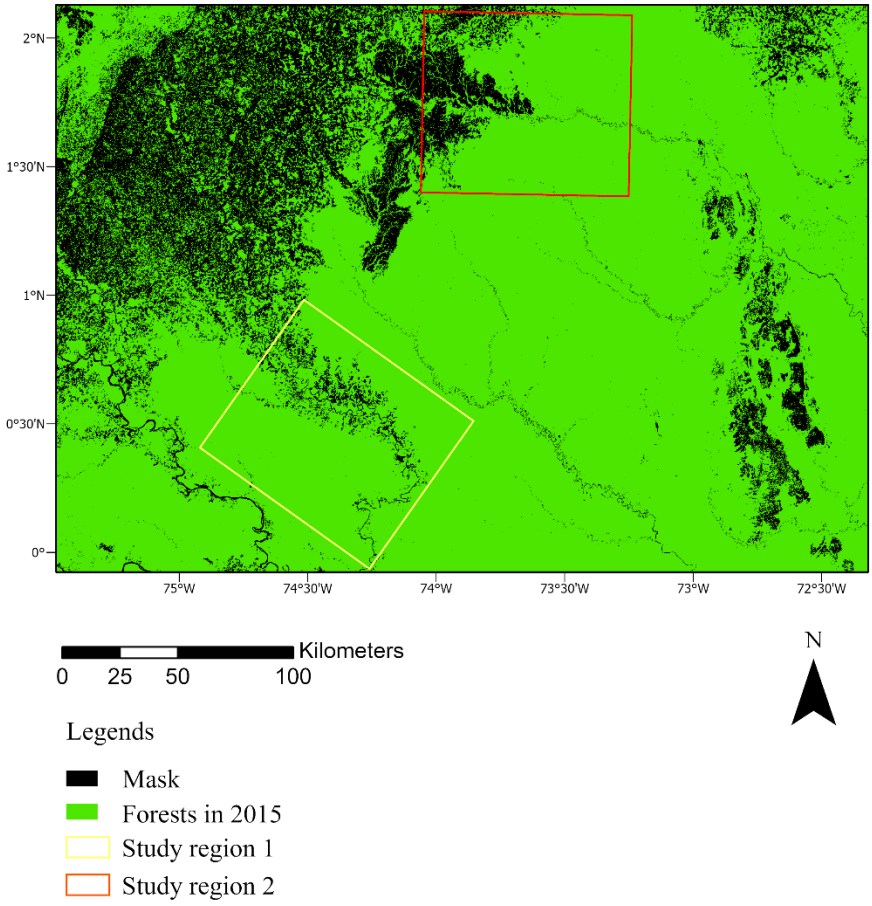

Figure 3. The forest mask covering two study regions in the northwest of the Colombian Amazon.

4 Methodology

This study used the CCDC time series change detection algorithm to monitor forest cover loss in the two study areas over a prolonged series and extract information on the deforestation dynamics. High-resolution remote sensing images from PlanetScope were used for visual interpretation to validate the accuracy of detected deforestation in the study regions. The applicability of Landsat and Sentinel-1 data was compared and analyzed from two key aspects: deforestation identification and deforestation time. The overall flow chart is shown in Figure 4.

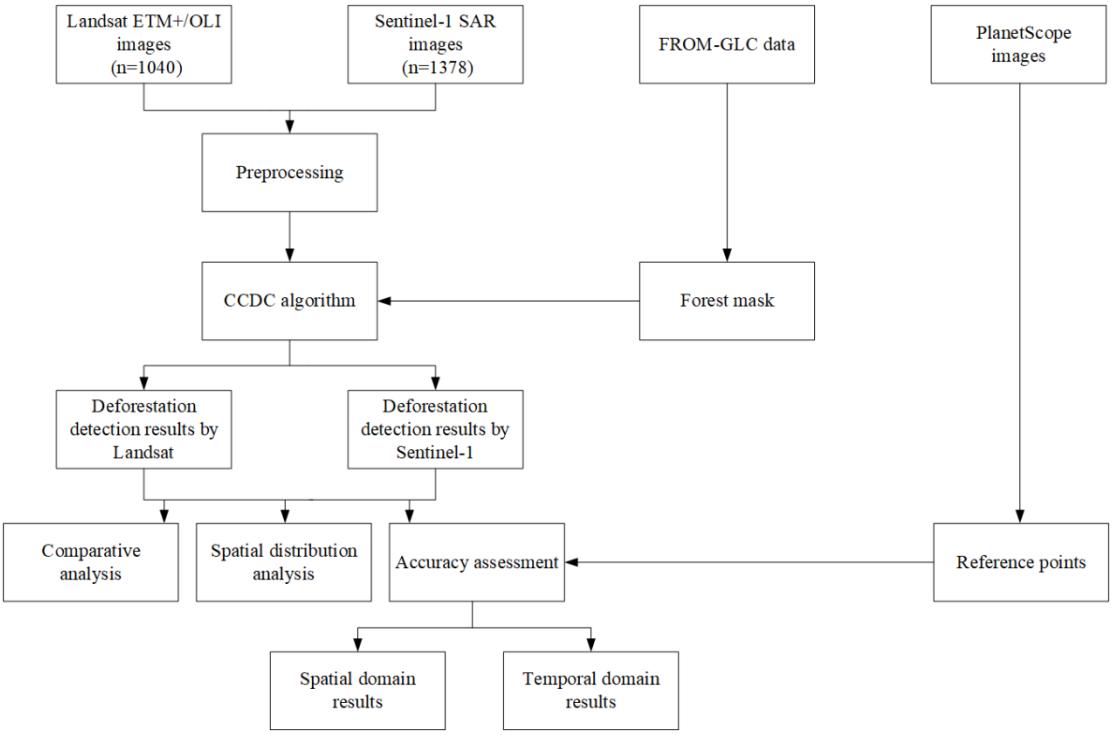

Figure 4. Flow chart of the methodology for the monitoring of deforestation using CCDC algorithm and Landsat, Sentinel-1 data.

4.1 The CCDC time series model

CCDC applies harmonic regression models (Eq.2) to each spectral band present in the time series data to capture intra-annual, gradual inter-annual and abrupt changes (Zhu and Woodcock, 2014). The meaning of parameters in Eq.2 is explained in Table 5.

$$\hat{\rho}(i,x)_{OLS} = a_{0,i} + a_{1,i}\cos\left(\frac{2\pi}{T}x\right) + b_{1,i}\sin\left(\frac{2\pi}{T}x\right) + c_{1,i}x \quad \{\tau^*_{k-1} < x \leq \tau^*_k\} \quad (2)$$

Table 5. Harmonic regression model and its parameters in Eq.2.

Parameters	*Meaning*
x	Julian date
i	the ith band
T	number of days per year (T = 365)
$a_{0,i}$	coefficient for overall value for the ith band
$a_{1,i}\&b_{1,i}$	coefficients for intra-annual change for the ith band
$c_{1,i}$	coefficient for inter-annual change for the ith band
τ^*_k	the kth break points
$\hat{\rho}(i,x)_{OLS}$	predicted value for the ith band at Julian date x

For all bands contained in time series data, the Ordinary Least Squares (OLS) method (Eq.2) is utilized and the Root Mean Square Error (RMSE) is calculated for each

spectral band. The deviation between the model predictions and observations for each band is normalized by three times the RMSE. This is done because when there is a change in land cover, the spectral signals often differ from the model prediction by more than three times the RMSE (Zhu and Woodcock, 2014). As a result, the “three times the RMSE” criterion is used to detect deforestation for each pixel. By using the visualize CCDC products tool (Arévalo et al., 2020), it is convenient to analyze the time series data for a specific pixel and examine the temporal segments that were fitted to the data using the CCDC algorithm (Figure 5).

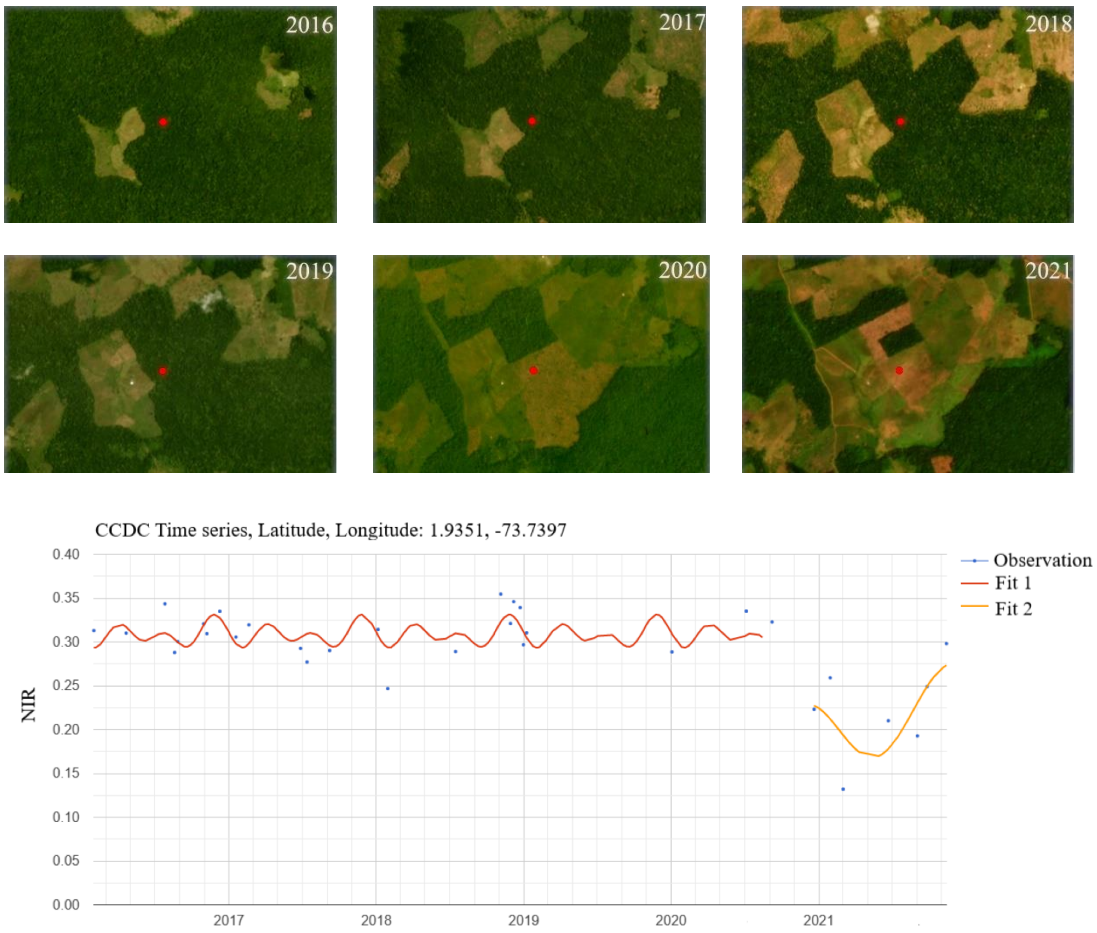

Figure 5. Example of rectangular patterns of deforestation identified in the 2016–2021 monitoring period. Above the time series plot, PlanetScope maps are provided for each year. The red point indicates the Landsat pixel for which the time series plot is displayed. The time series plot illustrates Landsat observations (blue dots) for the NIR band, along with the identified time segments (red line and yellow line) detected by the CCDC algorithm. The transition between time segment 1 and 2 represents a detected change in land cover.

4.2 Parameter settings of CCDC model in GEE

Initially, only users with adequate data storage and processing resources could employ CCDC, but with the development of cloud computing, now CCDC is available in GEE for implementation by a larger number of users (Pasquarella et al., 2022). With the necessary time-series image collection prepared and parameters set up in GEE, users can quickly obtain results of the CCDC algorithm. The following parameters were set for Landsat and Sentinel-1 images respectively (Table 6):

Table 6. CCDC parameters for Landsat and Sentinel-1 images.

Input parameters	*Landsat*	*Sentinel-1*
collection	Landsat collection	Sentinel-1 collection
breakpointBands	Green, Red, NIR, SWIR1, SWIR2	VV, VH, CR, RVI
tmaskBands	Green, SWIR2	Null
minObservations	6	6
chiSquareProbability	0.99	0.99
minNumOfYearsScaler	1.33	1.33
dateFormat	1	1
lambda	0.002	20
maxIterations	25000	25000

For Landsat data, all bands except for the blue and surface temperature bands were used to detect breakpoints. Green and SWIR2 bands were applied to conduct TMask cloud detection (Zhu and Woodcock, 2014). The default value of 6 for 'minObservations' was chosen, as it specifies the number of sequential observations necessary to mark a change. The sensitivity of the CCDC algorithm to detect changes is governed by the default parameters of 'chiSquareProbability', set at 0.99. In other words, a lower 'chiSquareProbability' means more pixels will be identified as changes, better tolerating commission errors (Cohen et al., 2020). The 'minNumOfYearsScaler' represents factors determining the minimum number of years required to apply new fitting and the default value 1.33 was chosen. There are three different data formats to choose from: Julian days (0), fractional years (1) and Unix time in milliseconds (2). To understand results solidly and straightforward, fractional years were designated, as it expresses the dates of detected breakpoints in decimal form. Moreover, the parameter

lambda defines the degree of regularization. When the value of lambda is excessively high, the model may not adequately grasp the seasonal patterns in the data, leading to underfitting. Conversely, if lambda is set too low, the model may overfit and detect false changes more frequently (Awty-Carroll et al., 2019). The default value of lambda at 20 was adopted, but it was divided by 10000 to match the surface reflectance units. Finally, the default value of 'maxIterations' at 25000 was specified to control the curve fitting process. The main objective of this study is to detect deforestation using the CCDC algorithm, and as a result, most of the parameters were chosen to align with the default values in GEE. For detailed parameter descriptions, please see https://developers.google.com/earth-engine/apidocs/ee-algorithms-temporalsegmentation-ccdc.

For Sentinel-1 data, all original bands and derived indices were included to detect breakpoints. Due to SAR images being unaffected by clouds, it is unnecessary to do cloud detection. The remaining parameters were set the same as for Landsat images, except for lambda because there was no need to convert units.

4.3 Extract change information

The CCDC output consisted of an array image that contained the fitting coefficients of breakpointBands (Table 6) as well as information required to assess any changes. The information included the start and end date of each time segment (tStart and tEnd), the break date if a change occurred (tBreak), and the numerical value assigned to indicate the probability of change for each of the bands that were used for detecting changes. (changeProb) (Xu et al., 2021). A mask was created to identify all positions within the image array where breaks were detected within the study period and satisfied the criterion of having a change probability of 1. This procedure helped to eliminate any false breaks that may have been detected. Finally, the forest mask mentioned in section 3.2.4 was used to filter detected pixels by CCDC. It should be noted that to ensure uniformity in subsequent analysis, this research utilized the timing of the first

occurrence of deforestation for each pixel, as some pixels had multiple deforestation events (Li et al., 2023).

4.4 Analysis of identified deforestation

The area of detected deforestation by Landsat and Sentinel-1 data was compared based on the statistical analysis, targeting to evaluate the significance of the differences. Common methods used for comparing differences between measured values include paired-samples t-test and Wilcoxon test (Gaveau et al., 2009). The difference between the two methods is that the Wilcoxon test does not require the assumption of normal data. If the assumption of normality is violated, the reliability and validity of parametric tests (e.g. paired-samples t-test) may be compromised (Milien et al., 2021). Therefore, in this study, the Shapiro-Wilk method, was applied first to determine whether the data fits a normal distribution. The method is commonly regarded as the most powerful test for assessing normality (Milien et al., 2021). Then, based on the results of the normality test, one of the methods, the paired-samples t-test or the Wilcoxon test, was chosen to investigate whether Landsat and Sentinel-1 generated statistically significant deforestation values in the results. This analysis was carried out by Statistical Package for the Social Sciences (SPSS).

In addition to the quantitative analysis of deforestation results, to investigate the directional trend of forest loss, calculations were performed to determine the standard deviation ellipses for each study area. The utilization of the standard deviation ellipse provides a valuable means to assess the spatial distribution of deforested regions (Achour et al., 2018). The standard deviation ellipses were generated in ArcGIS, with the ellipse size set to 1 standard deviation, which can encompass approximately 60% of the detected deforestation (Achour et al., 2018). The center of the elliptical surface is around the mean center of all detected deforestation from 2016 to 2021. The direction of the ellipse indicates the spatial distribution orientation of all deforested regions.

4.5 Validation

To evaluate the accuracy of change detection, a random stratified sample design was employed. In this context, validation represents an integral component of the process that provides a quantitative evaluation of whether the satellite observations are adequate for the intended use of the data in this study. By random stratified sampling, it is possible to adjust the sample size in classes that represent a small proportion of the total area. For instance, the forest loss during the period of 2016-2017 may be relatively infrequent compared to other study periods. This approach helps to minimize the standard errors associated with accuracy estimates specific to these fewer common classes (Olofsson et al., 2014). For the visual interpretation of the PlanetScope satellite imagery, a selection of 350 reference points was done for each study area (Figure 6). Among them, 50 points were derived from areas where no forest loss occurred between 2016 and 2021, while an additional 300 points were evenly distributed among the regions where forest loss occurred in each year from 2016 to 2021. The reason for not allocating samples proportionally is that it is not possible to accurately determine the ratio of forest disturbance to non-disturbance within the study area (Decuyper et al., 2022). Therefore, this research adopted the equal sample allocation strategy as previous studies (Jin et al., 2013; Zhu and Woodcock, 2014). The sample points were uniformly distributed within the research region. Each reference point indicates the actual time when deforestation occurred, or deforestation did not occur during the study period. The validation was conducted based on two aspects: whether forest cover loss was detected (spatial domain) and comparison of the actual time of forest loss with the time provided by CCDC (temporal domain). A confusion matrix and overall accuracy, producer's accuracy, and user's accuracy for spatial domain assessment were calculated. The widely used Kappa coefficient was not used to report the accuracy because it is relevant with overall accuracy and cannot provide useful information (Olofsson et al., 2014).

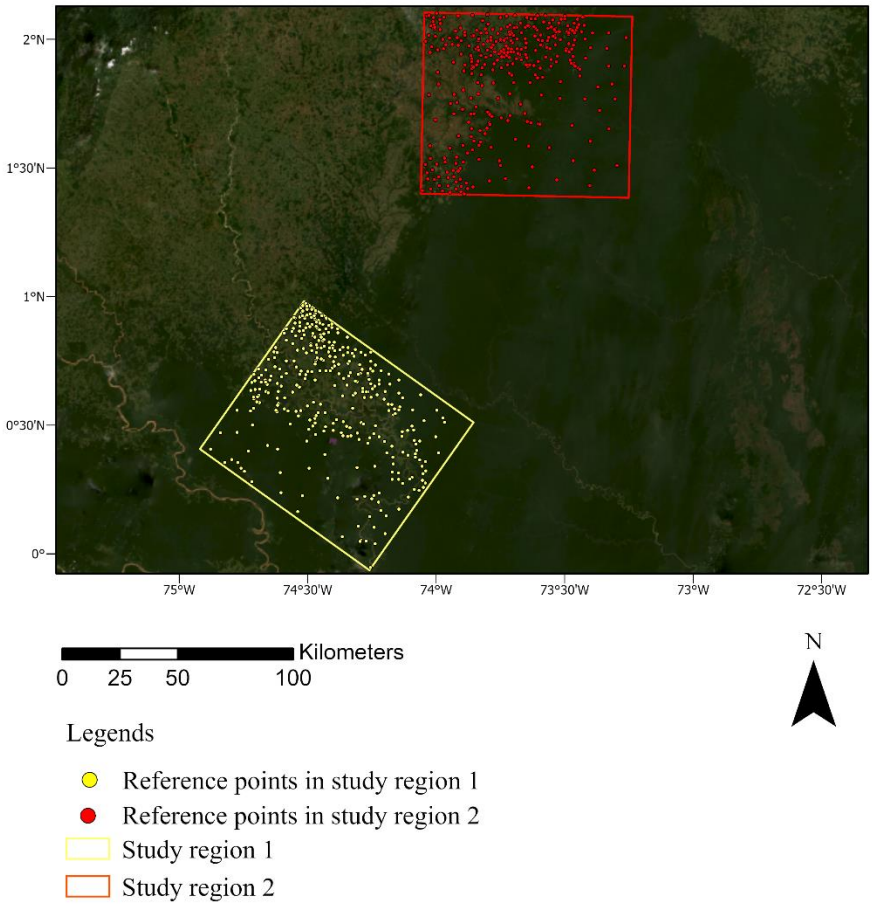

Figure 6. Visualization of the created reference points in the two study regions.

5 Results

5.1 Spatiotemporal distribution of the deforestation analysis

Following the proposed methodology, deforestation identification was performed in the two study regions using the CCDC algorithm. The detected deforestation of study region 1 and 2 and produced standard deviation ellipses are shown in Figure 7 and Figure 8, respectively. The background map is the PlanetScope visual monitoring mosaic image obtained in December 2021.

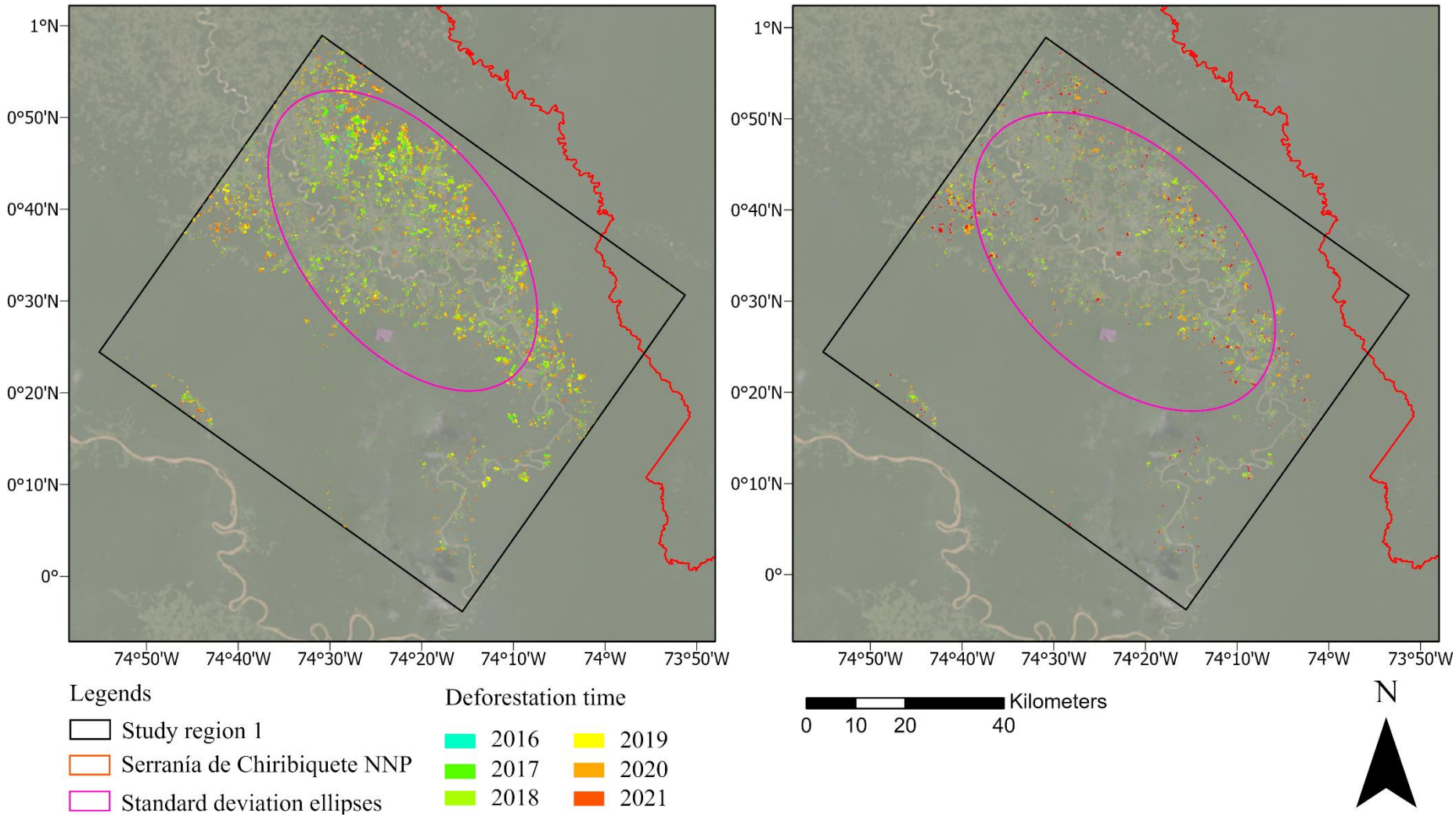

Figure 7. Detected deforestation and generated standard deviation ellipses in study region 1 using Landsat (left) and Sentinel-1 (right) data.

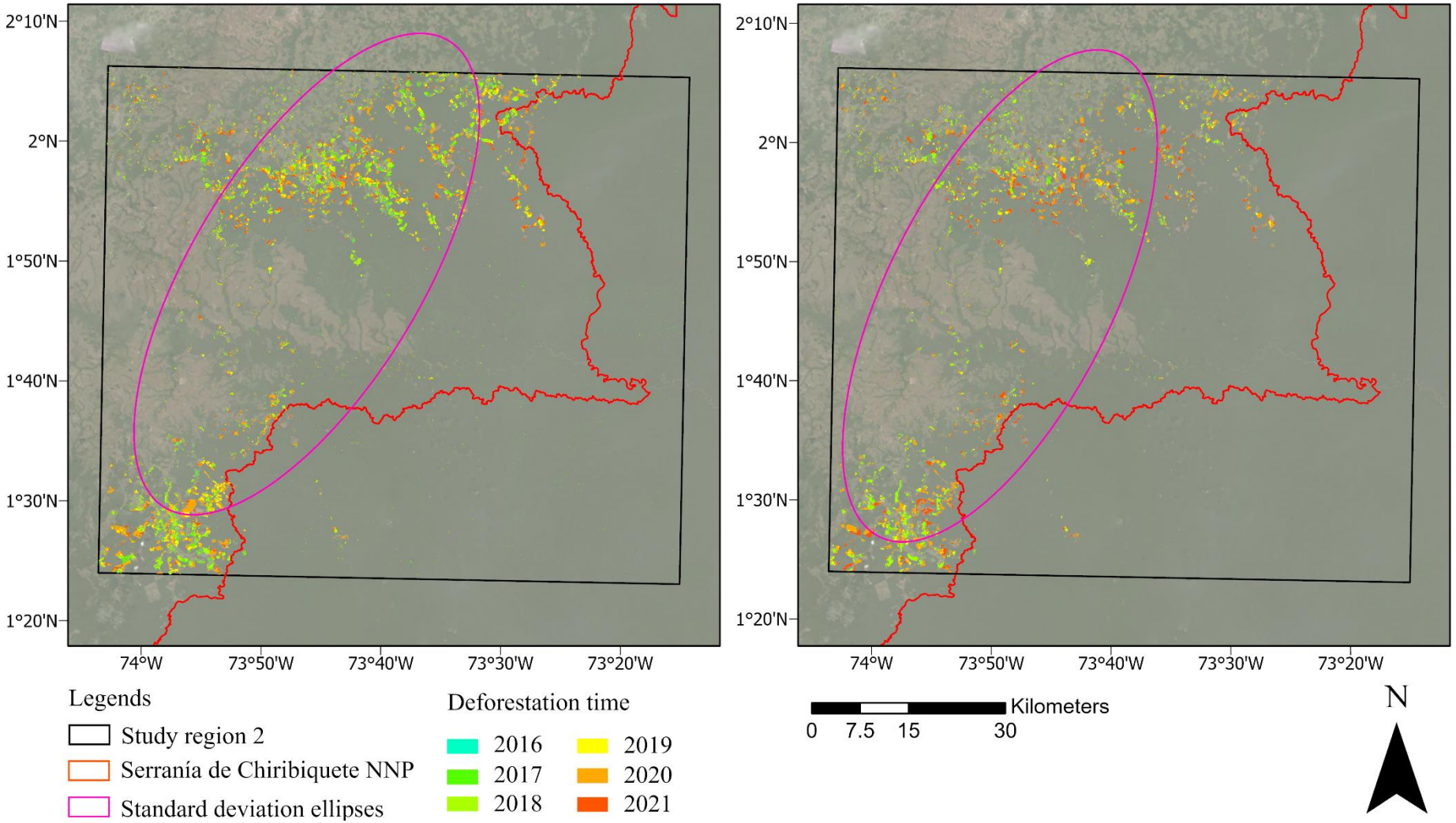

Figure 8. Detected deforestation and generated standard deviation ellipses in study region 2 using Landsat (left) and Sentinel-1 (right) data.

Statistics and differences on the annual deforestation area were calculated comparing the two regions (Table 7). The results shown in Table 7 explain that Landsat data always detected more deforestation events, compared with Sentinel-1 data. In study areas 1 and 2, Landsat detected approximately 60% and 30% more forest cover loss, respectively, compared to SAR. Also, in the two study regions, deforestation was detected at its lowest level in 2016, as this was the year when deforestation rates where at its lowest point during the peace accord process, with the armed groups controlling a vast portion of the area. Meanwhile, in study area 1, Landsat data detected the highest amount of deforestation in 2018, while Sentinel-1 data detected the highest amount in 2020. In study area 2, both Landsat and Sentinel-1 data detected the highest amount of deforestation in 2020.

Table 7. Area of deforestation (km^2) in study regions from 2016 to 2021.

		2016	2017	2018	2019	2020	2021	Total
Region 1	Landsat	6.352	48.459	99.687	49.625	82.481	30.597	317.201
	Sentinel-1	0.117	16.206	31.910	10.202	42.206	26.619	127.260
Region 2	Landsat	2.108	26.427	79.531	33.237	78.571	27.728	247.602
	Sentinel-1	0.000	8.823	49.825	20.258	55.685	34.655	169.246

The results of the Shapiro-Wilk test for the area of deforestation within the two study regions using Landsat and Sentinel-1 data, as shown in Table 7, indicate that all significance values are greater than 0.05 (Table 8). This suggests that the data conforms to a normal distribution. The following Paired-samples t-test shows that the difference between detected forest loss area by Landsat and Sentinel-1 data is statistically significant in region 1, while it is not statistically significant in region 2 (Table 8). In relation to the spatial distribution of deforestation, the four generated standard deviation ellipses indicate that deforestation in region 1 and 2 is concentrated in the northwest-southeast direction and the northeast-southwest direction, separately (Figure 7; Figure 8; Table 8). This is roughly consistent with the direction of the NNP boundary near the study area. Besides, it is evident that deforestation is very close to the boundary of the Serranía de Chiribiquete NNP, with development pushing towards the NNP border. In Figure 7 and Figure 8, deforestation activities were even detected within the NNP which indicates illegal forest cuttings inside protected areas.

Table 8. Comparative and spatial distribution analysis of detected deforestation by Landsat and Sentinel-1.

		Shapiro-Wilk test Significance	*Paired-samples t-test Significance*	*Rotation (°)*
Region 1	Landsat	0.882	0.023	140.833
	Sentinel-1	0.982		134.372
Region 2	Landsat	0.216	0.064	31.619
	Sentinel-1	0.697		26.694

5.2 Accuracy assessment of detected deforestation

By using selected reference points, the accuracy of the CCDC detected deforestation at any time during the study period was evaluated. Table 9 and Table 10 display the confusion matrix and user's, producer's, overall accuracy of the identified results with Landsat and Sentinel-1 data in both study regions, respectively.

Table 9. Confusion matrix of the identified results with Landsat data.

		Reference data			
		Deforestation	*No deforestation*	*Total*	*User's*
CCDC results	*Deforestation*	**339**	261	600	56.5%
	No deforestation	0	**100**	100	100%
	Total	339	361	**700**	
	Producer's	100%	27.7%	*Overall*	62.7%

Table 10. Confusion matrix of the identified results with Sentinel-1 data.

		Reference data			
		Deforestation	*No deforestation*	*Total*	*User's*
CCDC results	*Deforestation*	**203**	397	600	33.8%
	No deforestation	0	**100**	100	100%
	Total	203	497	**700**	
	Producer's	100%	20.1%	*Overall*	43.3%

As shown in Table 9 and Table 10, the overall accuracy for monitoring deforestation using Landsat and Sentinel-1 data is 62.7% and 43.3%, respectively. The overall accuracy of Sentinel-1 is 19.4% lower than that of Landsat. Furthermore, the producer's accuracy for deforestation with Landsat and Sentinel-1 data is significantly higher than the user's accuracy, indicating a higher occurrence of misclassifications than omissions. This means that the detected results erroneously identify areas with deforestation as areas without deforestation and the commission error is higher when using Sentinel-1. Thus, it shows that using Sentinel-1 data for deforestation detection may not be a good option, rather it can be use as complementary data to interpret the analysis along with Landsat data.

Table 11 illustrates the results of temporal accuracy of forest cover loss detection for pixels that are correctly identified as deforestation. The "temporal accuracy" refers to the percentage of pixels that have the same time of change in both the CCDC results and the reference data. The temporal accuracy of Landsat data is 62.8%, while that of Sentinel-1 data is 74.9%. Separately from this, for pixels which do not have the same time of change, Landsat data detected more deforestation earlier than actual time, while Sentinel-1 data tended to detect more deforestation in the later period than occurred.

Table 11. The evaluation of the accuracy of change detection over time.

	Same year	*Early*	*Late*	*Total*
Landsat	213	80	46	339
Proportion (%)	62.8	23.6	13.6	100
Sentinel-1	152	13	38	203
Proportion (%)	74.9	6.4	18.7	100

The evaluation of accuracy determines the quality of the information derived from the Landsat or Sentinel-1 remotely sensed data used to explore and detect deforestation in the study area.

6 Discussion

6.1 Deforestation change between 2016–2021

The reason for the continuous increase of deforestation in both study regions between 2016 and 2018 could have been influenced by the peace agreement signed in 2016 and its possible negative impact due to a lack of functional institutions in many protected areas and increase of cattle ranching in the Colombian Amazon (Ganzenmüller et al., 2022; Botero, R. 2022). Following the withdrawal of FARC in 2017, a significant surge in forest disturbance was apparent in 2018 and 2020 (Table 7).

Undeniably, NNP plays a significant role in reducing forest loss, as deforestation outside of NNP is considerably higher compared to within it. The establishment of NNP offers crucial protection against deforestation, aiding in the reduction of carbon emissions that contribute to climate change. (Milien et al., 2021). This study identified forest cover loss near and within the Serranía de Chiribiquete NNP, indicating a phenomenon that requires attention. Historically, the rate of forest disturbance within protected areas was relatively low (Murillo-Sandoval et al., 2020). However, due to the

transformation of the forest management framework after the armed conflict, the illegal land market was fueled, allowing participants to recoup their initial investments through cattle ranching or cultivating coca (Murillo-Sandoval et al., 2020). These activities resulted in severe deforestation, subsequently impacting climate change and the ecosystems of the Colombian Amazon forests. Although a well-organized governance framework for zero deforestation is planned to be established in Colombia, the enforcement of sanctions and laws continues to play a crucial role in mitigating the ongoing increase in deforestation following the conflict (Furumo et al., 2020).

In region 1, there is a statistically significant difference between the forest loss area detected by Landsat and Sentinel-1 data. However, in region 2, there is no statistically significant difference in the forest loss area detected by the two datasets. One possible explanation for this phenomenon could be that the number of used Sentinel-1 images in region 1 is higher than that of used images in region 2, resulting in more detected deforestation in region 1. In addition, geographical and environmental factors can contribute to variations in forest loss characteristics across different regions. These factors may include terrain, vegetation types, levels of forestry activities, and weather conditions. As a result, the ability of Landsat and Sentinel-1 data to detect forest loss may vary in different regions. Moreover, Landsat and Sentinel-1 are two different remote sensing data sources with distinct sensors, resolutions, and operational principles. Therefore, their capabilities in detecting forest loss may vary across different regions. Further research and analysis of these factors is needed to gain insight into the differences between Landsat and Sentinel-1 data in different regions and to provide better explanations for more accurate forest loss assessments.

6.2 Performance of the CCDC algorithm

The proportion of detected deforestation in 2016 by using Landsat and Sentinel-1 data is relatively low, compared with other years. A possible reason for this condition could be the lack of enough clear observations at the beginning of the model fitting period (Zhu and Woodcock, 2014). In addition, the number of obtained Sentinel-1 images in 2016 is the smallest, resulting in a forest cover loss area detected by Sentinel-1 in 2016 that is close to zero.

The CCDC algorithm uses an "online" method for segmentation, where observations are processed iteratively. Changing the start time of the input time series data can have a notable impact on the timing of the detected breakpoints, as well as the quality of the harmonic segments fitted to the data (Pasquarella et al., 2022). The comparison between the deforestation results obtained from long Landsat time series (2000-2021) and those from short Landsat time series (2016-2021) is illustrated in Figure 9. While utilizing longer Landsat time series can detect more instances of deforestation, one of the objectives of this study was to compare the accuracy of detected forest loss between Landsat and Sentinel-1 data. For this purpose, it is necessary to use data within the same time range. Due to the later launch of the Sentinel-1 satellites, it is important to mention that 2016 is considered in this study as the first year of reference for deforestation monitoring in the post-conflict situation of the region.

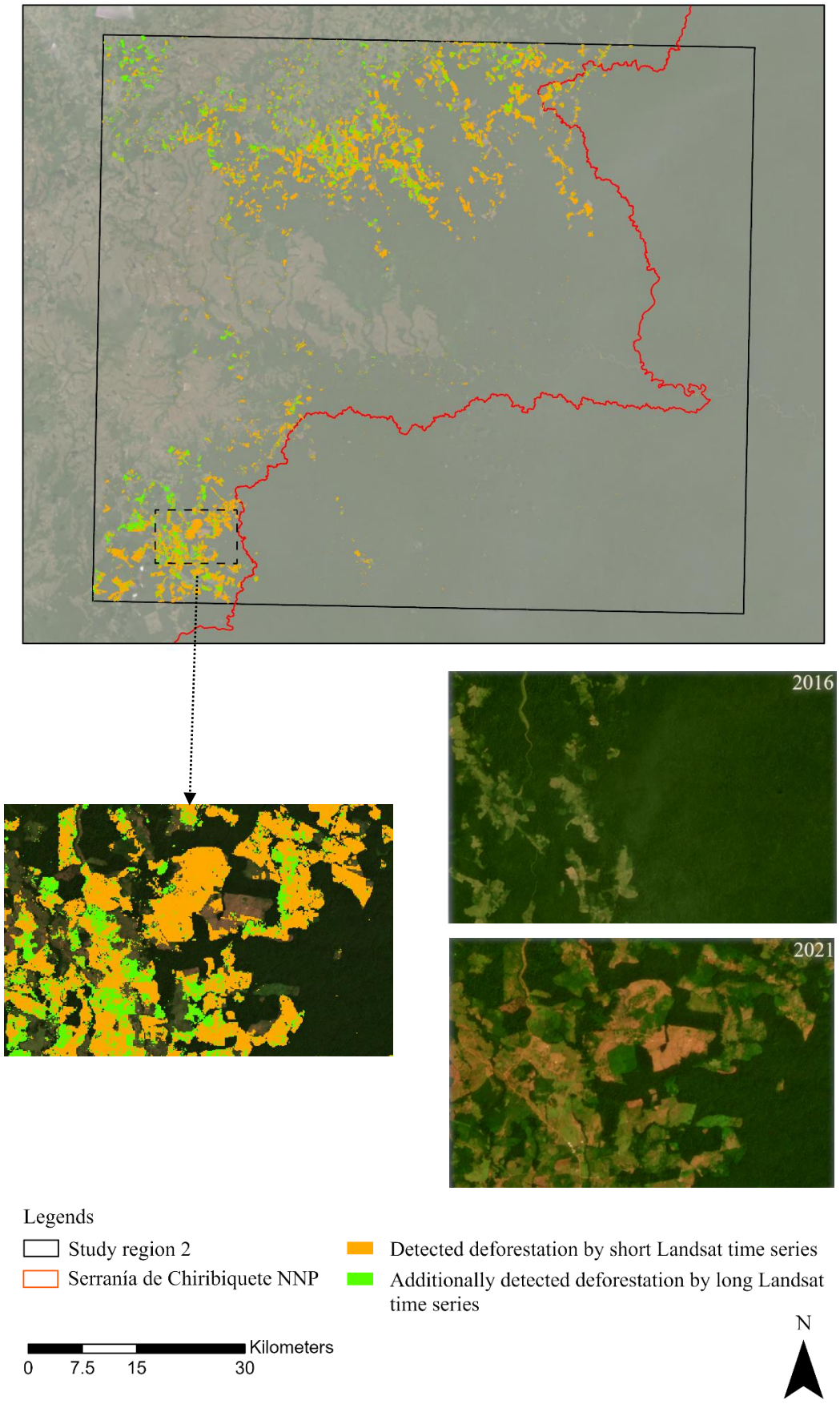

Figure 9. The comparison between the deforestation results obtained from long Landsat time series (2000-2021) and those from short Landsat time series (2016-

2021). One “snapshot” of the study region 2 highlights the difference of the CCDC results when changing the start time of the input time series. Two PlanetScope images beside the “snapshot” show the change of deforestation from 2016 to 2021.

From Figure 9, more pixels representing deforestation were detected and the pixel patches appeared more continuous when using longer Landsat time series data. To better evaluate the effect of using longer Landsat time series data, a comparison was carried out (Table 12) as it shows the significance of the time series method. The statistics indicate that using a longer time series causes a significant increase in detected forest cover loss during the first two years, with little variation in subsequent years. While CCDC aims to fit all the available observations for a particular pixel, it is important for users to consider the potential impact of temporal variability in observation frequency on the results (Pasquarella et al., 2022).

Table 12. Comparison of area of deforestation (km^2) in study region 2 between using long and short Landsat time series data.

Landsat data	*2016*	*2017*	*2018*	*2019*	*2020*	*2021*	*Total*
Long time series	28.140	58.037	85.159	33.797	77.848	25.940	308.921
Short time series	2.108	26.427	79.531	33.237	78.571	27.728	247.602
Difference	26.032	31.610	5.628	0.560	-0.723	-1.788	61.139

Furthermore, Landsat data detected more deforestation earlier than actual time, this could be attributed to overfitting. Overfitting can lead to significant issues even when utilizing basic time series models. This is particularly true in situations where the data is consistently absent during a specific time of year due to factors such as clouds (Zhu and Woodcock, 2014). Figure 10 illustrates how overfitting causes the CCDC model to detect the breakpoint ahead of time. In other tropical regions with more cloud cover, the implications of overfitting can be significant. Insufficient clear observations may produce inaccurate timing of deforestation, which can impact decision-making for forest conservation and sustainable management.

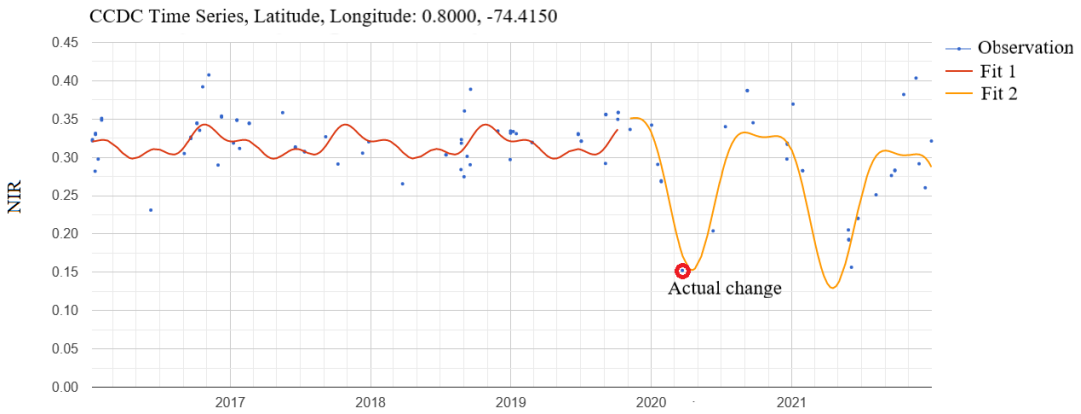

Figure 10. An example of overfitting of the CCDC time series model. The time series plot illustrates Landsat observations (blue dots) for the NIR band, along with the identified time segments (red line and yellow line) detected by the CCDC algorithm. The transition between time segment 1 and 2 indicates deforestation occurred in 2019. The red circle illustrates the correct assignment of change which happened in 2020.

6.3 Performance of Sentinel-1 data

Compared with Landsat data, the area and overall accuracy of detected deforestation by Sentinel-1 data is lower, indicating poorer performance (Table 7; Table 9; Table 10). Despite the low temporal resolution of Sentinel-1 data, the main shortcoming of C-band SAR data is short wavelength, and it is considered less suitable for detecting deforestation because C-band is more sensitive to fluctuations in surface moisture (Reiche et al.,2021) and the influences are larger in VH polarization compared with VV polarization (Benninga et al., 2019). Rainfall can cause soil moisture to increase, resulting in stronger backscattered signals. This effect can make it difficult to detect deforested areas, especially during prolonged rainfall events (Dascălu et al., 2023). Due to the study area being a tropical rainforest, this could explain why the performance of detecting deforestation using the Sentinel-1 data is unsatisfying and 18.7% of identified forest loss by Sentinel-1 data is later than occurred. One possible method to solve this problem is to extract seasonal signals in backscatter (Hethcoat et al., 2021) and future studies could be carried on that prospect. Meanwhile, longer time series should be applied because when using short time series, the seasonal variation may cause only a minor decrease of backscatter intensity (Dascălu et al., 2023).

6.4 Limitation and outlook of the Study

Particularly for this study, there are also some shortcomings. For example, the influence

of the used bands to detect breakpoints on the CCDC results was not investigated. In addition, the most crucial parameters that require determination may be the number of observations needed to indicate a change and the chi-square probability threshold for detecting changes, as well as the representativeness of selected areas to study within the larger area of the Amazonian arc of deforestation. The effect of these two parameters was also not studied. Further research is necessary to determine more appropriate parameter values for the selected study area and fulfilment of the research objectives.

The ongoing development and refinement of time series change detection algorithms and their implementations have created opportunities to improve results by combining multiple algorithms (Pasquarella et al., 2022). For example, fusing CCDC, Cumulative Sum of Residuals (CUSUM) and the Chow Test methods could decrease the commission and omission errors, compared with applying only one algorithm (Bullock et al., 2020). The drawback of this ensemble algorithm will result in the increase of computational requirements. However, combining the CCDC algorithm with the CUSUM is comparable to the 'BFASTmonitor' function in the 'BFAST' R package which could be implemented on GEE (Bullock et al., 2020; Hamunyela et al., 2020). Running the integrated algorithm on GEE saves time and storage space for data downloading and enables faster generation of results over a large area. This is only beneficial to remote sensing studies as an effective way in activating large-scale heterogeneous data to help monitor deforestation rates in tropical ecosystems now and in the future.

Additionally, data fusion is also a future research direction. Recently a new harmonized dataset of Landsat and Sentinel-2 imagery was applied to detect tropical forest disturbance in Tanzania and Brazil (Chen et al., 2021). The result showed combining Landsat and Sentinel- 2 could improve spatiotemporal accuracy compared with using Landsat or Sentinel-2 only (Chen et al., 2021). Except for fusing optical data, combining SAR time series with Landsat could also lead to better results of detected deforestation (Reiche et al., 2018). Although applying Sentinel-1 alone has not performed satisfactorily, a past study showed that Sentinel-1 can provide unprecedented potential in terms of dense observation and compensation for sudden environmental changes (Reiche et al., 2018). In addition, this study found that utilizing Sentinel-1 data

to detect deforestation could get better temporal accuracy. Therefore, fusing optical and SAR data could be a choice for future research. With the successful launch of Landsat-9 satellite in 2021 and the planned continuation of Sentinel-1 mission (including C and D), users can expect to access more frequent observations of optical data and C-band SAR data, providing an opportunity to further improvement of the accuracy of forest disturbance detection by fusing these types of data. (Masek et al., 2020; Hethcoat et al., 2021).

7 Conclusion

The Picachos-Tinigua-Macarena-Chiribiquete corridor holds significant importance within the Colombian Amazon region, as it is located in the Andes-Amazonian transition zone, important for movement of fauna and flora species, as well for the regulation of important hydrological processes taking place in this part of the Amazon biome. Understanding the forest loss in this corridor after the signing of the peace agreement is crucial for formulating sustainable forest management strategies that safeguard natural resources and the importance of its conservation, for better planning of the agricultural expansion process taking place.

This study applied the CCDC time series change detection method to distinguish deforestation by Landsat and Sentinel-1 data in northern and southern of the Serranía de Chiribiquete NNP from the period between 2016 and 2021. The results indicate that the deforestation area in both study areas gradually increased from 2016 to 2018, followed by a fluctuating trend. The peak periods of forest loss occurred in 2018 and 2020. Furthermore, the spatial distribution analysis of deforestation revealed that the detected forest cuttings within the two study areas from 2016 to 2021 exhibited a similar directional pattern to the boundaries of the Serranía de Chiribiquete NNP. The illegal deforestation was detected within the jurisdiction of the NNP, highlighting the need for concern in future land policies development.

The differences in detected deforestation area inside the two study areas between using Landsat and Sentinel-1 are not all statistically significant. The overall accuracy of identified forest cover loss indicated Landsat data performed better, compared with Sentinel-1 data. Moreso, extending the start time of used time series data could result

in changes of detected deforestation. From the aspect of temporal accuracy, Sentinel-1 data could achieve more accurate results. The reason for the early detection of forest cover loss detected by Landsat may be due to clouds, which caused unclear observation of the image, thus possibly triggering overfitting of the CCDC model. In summary, both Landsat and Sentinel-1 data can be used to detect deforestation based on the CCDC algorithm. When users seek results over a long time range, Landsat is a better choice due to its long historical archive. Compared to users' way to detect deforestation in the short term, fusing Landsat and Sentinel-1 might be a better option which may obtain results with good spatial and temporal accuracy.

With the availability of more dense time series data from Landsat, Sentinel-1, or other sensors in the future, the fusion of different types of data can enhance the capability of detecting forest loss in tropical areas. Apart from data combination, using ensemble time series methods could also be a future research direction. As more and more change detection algorithms are being implemented in GEE, there are now greater possibilities to evaluate these algorithms separately and in combination for a wide range of potential applications. Interestingly, recent developments using 3m resolution satellite imagery from Planet Labs are generating very high-resolution composites covering continental Africa (Reiner et al., 2023), which could benefit the scientific contributions of these applications of remote sensing in tropical ecosystems like the Amazon biome.

References

Achour, H., Toujani, A., Rzigui, T., & Faïz, S. (2018). Forest cover in Tunisia before and after the 2011 Tunisian revolution: a spatial analysis approach. *Journal of Geovisualization and Spatial Analysis*, *2*, 1-14. https://doi.org/10.1007/s41651-018-0017-7

Arévalo, P., Bullock, E. L., Woodcock, C. E., & Olofsson, P. (2020). A suite of tools for continuous land change monitoring in google earth engine. Frontiers in Climate, 2, 576740. https://doi.org/10.3389/fclim.2020.576740

Arias-Gaviria, J., Suarez, C. F., Marrero-Trujillo, V., Villegas-Palacio, C., & Arango-Aramburo, S. (2021). Drivers and effects of deforestation in Colombia: a systems thinking approach. *Regional Environmental Change*, *21*(4), 1-14. https://doi.org/10.1007/s10113-021-01822-x

Awty-Carroll, K., Bunting, P., Hardy, A., & Bell, G. (2019). Using continuous change detection and classification of Landsat data to investigate long-term mangrove dynamics in the Sundarbans region. *Remote Sensing*, *11*(23), 2833. https://doi.org/10.3390/rs11232833

Banskota, A., Kayastha, N., Falkowski, M. J., Wulder, M. A., Froese, R. E., & White, J. C. (2014). Forest monitoring using Landsat time series data: A review. *Canadian Journal of Remote Sensing*, *40*(5), 362-384. https://doi.org/10.1080/07038992.2014.987376

Benninga, H. J. F., van der Velde, R., & Su, Z. (2019). Impacts of radiometric uncertainty and weather-related surface conditions on soil moisture retrievals with Sentinel-1. *Remote sensing*, *11*(17), 2025. https://doi.org/10.3390/rs11172025

Botero, R. 2022. Webinar: Combating loss of connectivity in the arc of deforestation in Colombia. A visit to non-sustainable cattle ranching. October 6th of 2022. Lund University. Arranged by Jesica López.

Bouvet, A., Mermoz, S., Ballère, M., Koleck, T., & Le Toan, T. (2018). Use of the SAR shadowing effect for deforestation detection with Sentinel-1 time series. *Remote Sensing*, *10*(8), 1250.https://doi.org/10.3390/rs10081250

Brovelli, M. A., Sun, Y., & Yordanov, V. (2020). Monitoring forest change in the amazon using multi-temporal remote sensing data and machine learning classification on Google Earth Engine. *ISPRS International Journal of Geo-Information*, *9*(10), 580.https://doi.org/10.3390/ijgi9100580

Bullock, E. L., Healey, S. P., Yang, Z., Houborg, R., Gorelick, N., Tang, X., & Andrianirina, C. (2022). Timeliness in forest change monitoring: A new assessment framework demonstrated using Sentinel-1 and a continuous change detection algorithm. *Remote Sensing of Environment*, *276*, 113043. https://doi.org/10.1016/j.rse.2022.113043

Bullock, E. L., Woodcock, C. E., & Holden, C. E. (2020). Improved change monitoring using an ensemble of time series algorithms. *Remote Sensing of Environment*, *238*, 111165.https://doi.org/10.1016/j.rse.2019.04.018

Bullock, E. L., Woodcock, C. E., & Olofsson, P. (2020). Monitoring tropical forest degradation using spectral unmixing and Landsat time series analysis. *Remote sensing of Environment*, *238*, 110968.https://doi.org/10.1016/j.rse.2018.11.011

Chen, N., Tsendbazar, N. E., Hamunyela, E., Verbesselt, J., & Herold, M. (2021). Sub-

annual tropical forest disturbance monitoring using harmonized Landsat and Sentinel-2 data. *International Journal of Applied Earth Observation and Geoinformation*, *102*, 102386.https://doi.org/10.1016/j.jag.2021.102386

Clerici, N., Armenteras, D., Kareiva, P., Botero, R., Ramírez-Delgado, J. P., Forero-Medina, G., ... & Biggs, D. (2020). Deforestation in Colombian protected areas increased during post-conflict periods. *Scientific reports*, *10*(1), 1-10. https://doi.org/10.1038/s41598-020-61861-y

Clerici, N., Salazar, C., Pardo-Díaz, C., Jiggins, C. D., Richardson, J. E., & Linares, M. (2019). Peace in Colombia is a critical moment for Neotropical connectivity and conservation: Save the northern Andes–Amazon biodiversity bridge. *Conservation Letters*, *12*(1), e12594. https://doi.org/10.1111/conl.12594

Cohen, W. B., Healey, S. P., Yang, Z., Zhu, Z., & Gorelick, N. (2020). Diversity of algorithm and spectral band inputs improves Landsat monitoring of forest disturbance. *Remote Sensing*, *12*(10), 1673.https://doi.org/10.3390/rs12101673

Dascălu, A., Catalão, J., & Navarro, A. (2023). Detecting Deforestation Using Logistic Analysis and Sentinel-1 Multitemporal Backscatter Data. *Remote Sensing*, *15*(2), 290.https://doi.org/10.3390/rs15020290

Decuyper, M., Chávez, R. O., Lohbeck, M., Lastra, J. A., Tsendbazar, N., Hackländer, J., ... & Vågen, T. G. (2022). Continuous monitoring of forest change dynamics with satellite time series. *Remote Sensing of Environment*, *269*, 112829.https://doi.org/10.1016/j.rse.2021.112829

DeVries, B., Verbesselt, J., Kooistra, L., & Herold, M. (2015). Robust monitoring of small-scale forest disturbances in a tropical montane forest using Landsat time series. *Remote Sensing of Environment*, *161*, 107-121. https://doi.org/10.1016/j.rse.2015.02.012

Di Maio Mantovani, A. C., & Setzer, A. W. (1997). Deforestation detection in the Amazon with an AVHRR-based system. International Journal of Remote Sensing, 18(2), 273-286.https://doi.org/10.1080/014311697219060

Doblas, J., Shimabukuro, Y., Sant'Anna, S., Carneiro, A., Aragão, L., & Almeida, C. (2020). Optimizing near real-time detection of deforestation on tropical rainforests using sentinel-1 data. *Remote Sensing*, *12*(23), 3922. https://doi.org/10.3390/rs12233922

Drusch, M., Del Bello, U., Carlier, S., Colin, O., Fernandez, V., Gascon, F., ... & Bargellini, P. (2012). Sentinel-2: ESA's optical high-resolution mission for GMES operational services. *Remote sensing of Environment*, *120*, 25-36. https://doi.org/10.1016/j.rse.2011.11.026

Finer, M., & Mamani, N. (2020). MAAP Synthesis: 2019 Amazon Deforestation Trends and Hotspots. *MAAP Synthesis*, *4*. Available at: https://www.amazonconservation.org/tag/synthesis

Foga, S., Scaramuzza, P. L., Guo, S., Zhu, Z., Dilley Jr, R. D., Beckmann, T., ... & Laue, B. (2017). Cloud detection algorithm comparison and validation for operational Landsat data products. *Remote sensing of environment*, *194*, 379-390.https://doi.org/10.1016/j.rse.2017.03.026

Francini, S., McRoberts, R. E., Giannetti, F., Mencucci, M., Marchetti, M., Scarascia Mugnozza, G., & Chirici, G. (2020). Near-real time forest change detection using PlanetScope imagery. *European Journal of Remote Sensing*, *53*(1), 233-244.https://doi.org/10.1080/22797254.2020.1806734

Fu, B., Lan, F., Yao, H., Qin, J., He, H., Liu, L., ... & Gao, E. (2022). Spatio-temporal monitoring of marsh vegetation phenology and its response to hydro-

meteorological factors using CCDC algorithm with optical and SAR images: In case of Honghe National Nature Reserve, China. *Science of The Total Environment*, *843*, 156990.https://doi.org/10.1016/j.scitotenv.2022.156990

Fu, P., & Weng, Q. (2016). A time series analysis of urbanization induced land use and land cover change and its impact on land surface temperature with Landsat imagery. *Remote sensing of Environment*, *175*, 205-214. https://doi.org/10.1016/j.rse.2015.12.040

Furumo, P. R., & Lambin, E. F. (2020). Scaling up zero-deforestation initiatives through public-private partnerships: A look inside post-conflict Colombia. *Global Environmental Change*, *62*, 102055. https://doi.org/10.1016/j.gloenvcha.2020.102055

Ganzenmüller, R., Sylvester, J. M., & Castro-Nunez, A. (2022). What peace means for deforestation: An analysis of local deforestation dynamics in times of conflict and peace in Colombia. *Frontiers in Environmental Science*, *10*, 51. https://doi.org/10.3389/fenvs.2022.803368

Gaveau, D. L., Epting, J., Lyne, O., Linkie, M., Kumara, I., Kanninen, M., & Leader-Williams, N. (2009). Evaluating whether protected areas reduce tropical deforestation in Sumatra. *Journal of biogeography*, *36*(11), 2165-2175. https://doi.org/10.1111/j.1365-2699.2009.02147.x

Gong, P., Wang, J., Yu, L., Zhao, Y., Zhao, Y., Liang, L., ... & Chen, J. (2013). Finer resolution observation and monitoring of global land cover: First mapping results with Landsat TM and ETM+ data. *International Journal of Remote Sensing*, *34*(7), 2607-2654.https://doi.org/10.1080/01431161.2012.748992

Guild, L. S., Cohen, W. B., & Kauffman, J. B. (2004). Detection of deforestation and land conversion in Rondonia, Brazil using change detection techniques. *International Journal of Remote Sensing*, *25*(4), 731-750. https://doi.org/10.1080/0143116031000159893 5

Hamunyela, E., Brandt, P., Shirima, D., Do, H. T. T., Herold, M., & Roman-Cuesta, R. M. (2020). Space-time detection of deforestation, forest degradation and regeneration in montane forests of Eastern Tanzania. *International Journal of Applied Earth Observation and Geoinformation*, *88*, 102063. https://doi.org/10.1016/j.jag.2020.102063

Hamunyela, E., Rosca, S., Mirt, A., Engle, E., Herold, M., Gieseke, F., & Verbesselt, J. (2020). Implementation of BFASTmonitor algorithm on google earth engine to support large-area and sub-annual change monitoring using earth observation data. *Remote Sensing*, *12*(18), 2953. https://doi.org/10.3390/rs12182953

Hansen, M. C., & Loveland, T. R. (2012). A review of large area monitoring of land cover change using Landsat data. *Remote sensing of Environment*, *122*, 66-74. https://doi.org/10.1016/j.rse.2011.08.024

Hansen, M. C., Potapov, P. V., Moore, R., Hancher, M., Turubanova, S. A., Tyukavina, A., ... & Townshend, J. (2013). High-resolution global maps of 21st-century forest cover change. *science*, *342*(6160), 850-853. https://doi.org/10.1126/science.1244693

Harris, N. L., Gibbs, D. A., Baccini, A., Birdsey, R. A., De Bruin, S., Farina, M., ... & Tyukavina, A. (2021). Global maps of twenty-first century forest carbon fluxes. *Nature Climate Change, 11*(3), 234-240. https://doi.org/10.1038/s41558-020-00976-6

Hethcoat, M. G., Carreiras, J. M., Edwards, D. P., Bryant, R. G., & Quegan, S. (2021). Detecting tropical selective logging with C-band SAR data may require a time

series approach. *Remote Sensing of Environment*, *259*, 112411.https://doi.org/10.1016/j.rse.2021.112411

Isaienkov, K., Yushchuk, M., Khramtsov, V., & Seliverstov, O. (2020). Deep learning for regular change detection in Ukrainian forest ecosystem with sentinel-2. *IEEE Journal of Selected Topics in Applied Earth Observations and Remote Sensing*, *14*, 364-376. https://doi.org/10.1109/JSTARS.2020.3034186

Jin, S., Yang, L., Danielson, P., Homer, C., Fry, J., & Xian, G. (2013). A comprehensive change detection method for updating the National Land Cover Database to circa 2011. *Remote sensing of environment*, *132*, 159-175. https://doi.org/10.1016/j.rse.2013.01.012

Joshi, N., Baumann, M., Ehammer, A., Fensholt, R., Grogan, K., Hostert, P., ... & Waske, B. (2016). A review of the application of optical and radar remote sensing data fusion to land use mapping and monitoring. Remote Sensing, 8(1), 70. https://doi.org/10.3390/rs8010070

Landsat Missions. (n.d.). Landsat Collection 2. Landsat Missions. Retrieved March 21, 2023, from https://www.usgs.gov/landsat-missions/landsat-collection-2

Lichun, S. (2009). Active Radar and Lidar Remote Sensing [M]. *Surveying and Mapping Press*.

Li, J., Zhang, Y., Zhang, C., Xie, H., Zhang, C., Du, M., & Wang, Y. (2023). Applicability Analysis of LandTrendr and CCDC Algorithms for Vegetation Damage Identification in Shendong Coal Base. *Metal Mine*, *01*, 55-64. https://doi.org/10.19614/j.cnki.jsks.202301006

Lohberger, S., Stängel, M., Atwood, E. C., & Siegert, F. (2018). Spatial evaluation of Indonesia's 2015 fire-affected area and estimated carbon emissions using Sentinel-1. *Global change biology*, *24*(2), 644-654. https://doi.org/10.1111/gcb.13841

Mandal, D., Kumar, V., Ratha, D., Dey, S., Bhattacharya, A., Lopez-Sanchez, J. M., ... & Rao, Y. S. (2020). Dual polarimetric radar vegetation index for crop growth monitoring using sentinel-1 SAR data. *Remote Sensing of Environment*, *247*, 111954.https://doi.org/10.1016/j.rse.2020.111954

Masek, J. G., Vermote, E. F., Saleous, N. E., Wolfe, R., Hall, F. G., Huemmrich, K. F., ... & Lim, T. K. (2006). A Landsat surface reflectance dataset for North America, 1990-2000. *IEEE Geoscience and Remote sensing letters*, *3*(1), 68-72. http://dx.doi.org/10.1109/LGRS.2005.857030

Milien, E. J., da Silva Rocha, K., Brown, I. F., & Perz, S. G. (2021). Roads, deforestation and the mitigating effect of the Chico Mendes extractive reserve in the southwestern Amazon. *Trees, Forests and People*, *3*, 100056. https://doi.org/10.1016/j.tfp.2020.100056

Masek, J. G., Wulder, M. A., Markham, B., McCorkel, J., Crawford, C. J., Storey, J., & Jenstrom, D. T. (2020). Landsat 9: Empowering open science and applications through continuity. *Remote Sensing of Environment*, *248*, 111968. https://doi.org/10.1016/j.rse.2020.111968

Ministerio de Medio Ambiente y Dessarollo Sostenible (MADS). (2020). Ficha técnica Parque Nacional Natural Serranía de Chiribiquete. Available at: https://www.parquesnacionales.gov.co/portal/es/parques-nacionales/parque-nacional-natural-chiribiquete/

Morton, D. C., DeFries, R. S., Shimabukuro, Y. E., Anderson, L. O., Del Bon Espírito-Santo, F., Hansen, M., & Carroll, M. (2005). Rapid assessment of annual deforestation in the Brazilian Amazon using MODIS data. *Earth Interactions*, *9*(8), 1-22. https://doi.org/10.1175/EI139.1

Mullissa, A., Vollrath, A., Odongo-Braun, C., Slagter, B., Balling, J., Gou, Y., ... & Reiche, J. (2021). Sentinel-1 sar backscatter analysis ready data preparation in google earth engine. *Remote Sensing*, *13*(10), 1954. https://doi.org/10.3390/rs13101954

Murillo-Sandoval, P. J., Clerici, N., & Correa-Ayram, C. (2022). Rapid loss in landscape connectivity after the peace agreement in the Andes-Amazon region. *Global Ecology and Conservation*, *38*, e02205. https://doi.org/10.1016/j.gecco.2022.e02205

Murillo-Sandoval, P. J., Van Dexter, K., Van Den Hoek, J., Wrathall, D., & Kennedy, R. (2020). The end of gunpoint conservation: Forest disturbance after the Colombian peace agreement. *Environmental Research Letters*, *15*(3), 034033. https://doi.org/10.1088/1748-9326/ab6ae3

Nasirzadehdizaji, R., Balik Sanli, F., Abdikan, S., Cakir, Z., Sekertekin, A., & Ustuner, M. (2019). Sensitivity analysis of multi-temporal Sentinel-1 SAR parameters to crop height and canopy coverage. *Applied Sciences*, *9*(4), 655. https://doi.org/10.3390/app9040655

NICFI. (2021). NICFI Program - Satellite Imagery and Monitoring —Planet. Retrieved March 21, 2023, from https://www.planet.com/nicfi/

Olofsson, P., Foody, G. M., Herold, M., Stehman, S. V., Woodcock, C. E., & Wulder, M. A. (2014). Good practices for estimating area and assessing accuracy of land change. *Remote sensing of Environment*, *148*, 42-57. https://doi.org/10.1016/j.rse.2014.02.015

Pasquarella, V. J., Arévalo, P., Bratley, K. H., Bullock, E. L., Gorelick, N., Yang, Z., & Kennedy, R. E. (2022). Demystifying LandTrendr and CCDC temporal segmentation. *International Journal of Applied Earth Observation and Geoinformation*, *110*, 102806. https://doi.org/10.1016/j.jag.2022.102806

Quegan, S., & Yu, J. J. (2001). Filtering of multichannel SAR images. *IEEE Transactions on geoscience and remote sensing*, *39*(11), 2373-2379. https://doi.org/10.1109/36.964973

Reiche, J., Hamunyela, E., Verbesselt, J., Hoekman, D., & Herold, M. (2018). Improving near-real time deforestation monitoring in tropical dry forests by combining dense Sentinel-1 time series with Landsat and ALOS-2 PALSAR-2. *Remote Sensing of Environment*, *204*, 147-161. https://doi.org/10.1016/j.rse.2017.10.034

Reiche, J., Mullissa, A., Slagter, B., Gou, Y., Tsendbazar, N. E., Odongo-Braun, C., ... & Herold, M. (2021). Forest disturbance alerts for the Congo Basin using Sentinel-1. *Environmental Research Letters*, *16*(2), 024005. https://doi.org/10.1088/1748-9326/abd0a8

Reiche, J., Verhoeven, R., Verbesselt, J., Hamunyela, E., Wielaard, N., & Herold, M. (2018). Characterizing tropical forest cover loss using dense Sentinel-1 data and active fire alerts. *Remote Sensing*, *10*(5), 777. https://doi.org/10.3390/rs10050777

Reiner, F., Brandt, M., Tong, X., Skole, D., Kariryaa, A., Ciais, P., ... & Fensholt, R. (2023). More than one quarter of Africa's tree cover is found outside areas previously classified as forest. *Nature Communications*, *14*(1), 2258.https://doi.org/10.1038/s41467-023-37880-4

Seymour, F., & Busch, J. (2016). *Why forests? Why now?: The science, economics, and politics of tropical forests and climate change*. Brookings Institution Press.

Schlund, M., & Erasmi, S. (2020). Sentinel-1 time series data for monitoring the

phenology of winter wheat. *Remote sensing of environment*, *246*, 111814. https://doi.org/10.1016/j.rse.2020.111814

Shimizu, K., Ota, T., & Mizoue, N. (2019). Detecting forest changes using dense Landsat 8 and Sentinel-1 time series data in tropical seasonal forests. *Remote Sensing*, *11*(16), 1899.https://doi.org/10.3390/rs11161899

Stasolla, M., & Neyt, X. (2018). An operational tool for the automatic detection and removal of border noise in Sentinel-1 GRD products. *Sensors*, *18*(10), 3454. https://doi.org/10.3390/s18103454

Tang, X., Bullock, E. L., Olofsson, P., Estel, S., & Woodcock, C. E. (2019). Near real-time monitoring of tropical forest disturbance: New algorithms and assessment framework. *Remote Sensing of Environment*, *224*, 202-218. https://doi.org/10.1016/j.rse.2019.02.003

Tsokas, A., Rysz, M., Pardalos, P. M., & Dipple, K. (2022). SAR data applications in earth observation: An overview. *Expert Systems with Applications*, 117342. https://doi.org/10.1016/j.eswa.2022.117342

Vermote, E., Justice, C., Claverie, M., & Franch, B. (2016). Preliminary analysis of the performance of the Landsat 8/OLI land surface reflectance product. *Remote Sensing of Environment*, *185*, 46-56. https://doi.org/10.1016/j.rse.2016.04.008

Vollrath, A., Mullissa, A., & Reiche, J. (2020). Angular-based radiometric slope correction for Sentinel-1 on google earth engine. Remote Sensing, 12(11), 1867. https://doi.org/10.3390/rs12111867

Vreugdenhil, M., Wagner, W., Bauer-Marschallinger, B., Pfeil, I., Teubner, I., Rüdiger, C., & Strauss, P. (2018). Sensitivity of Sentinel-1 backscatter to vegetation dynamics: An Austrian case study. *Remote Sensing*, *10*(9), 1396. https://doi.org/10.3390/rs10091396

Wagner, F. H., Dalagnol, R., Silva-Junior, C. H., Carter, G., Ritz, A. L., Hirye, M., ... & Saatchi, S. (2023). Mapping Tropical Forest Cover and Deforestation with Planet NICFI Satellite Images and Deep Learning in Mato Grosso State (Brazil) from 2015 to 2021. *Remote Sensing*, *15*(2), 521. https://doi.org/10.3390/rs15020521

Wulder, M. A., Roy, D. P., Radeloff, V. C., Loveland, T. R., Anderson, M. C., Johnson, D. M., ... & Cook, B. D. (2022). Fifty years of Landsat science and impacts. *Remote Sensing of Environment*, *280*, 113195. https://doi.org/10.1016/j.rse.2022.113195

Xu, H., Qi, S., Li, X., Gao, C., Wei, Y., & Liu, C. (2021). Monitoring three-decade dynamics of citrus planting in Southeastern China using dense Landsat records. *International Journal of Applied Earth Observation and Geoinformation*, *103*, 102518.https://doi.org/10.1016/j.jag.2021.102518

Ygorra, B., Frappart, F., Wigneron, J. P., Moisy, C., Catry, T., Baup, F., ... & Riazanoff, S. (2021). Monitoring loss of tropical forest cover from Sentinel-1 time-series: A CuSum-based approach. *International Journal of Applied Earth Observation and Geoinformation*, *103*, 102532. https://doi.org/10.1016/j.jag.2021.102532

Zhong, L., Chen, Y., & Wang, X. (2020). Forest disturbance monitoring based on time series of Landsat data. *Scientia Silvae Sinicae*, *56*(5), 80-88. https://doi.org/10.11707/j.1001-7488.20200509

Zhu, Z. (2017). Change detection using landsat time series: A review of frequencies, preprocessing, algorithms, and applications. *ISPRS Journal of Photogrammetry and Remote Sensing*, *130*, 370-384.

https://doi.org/10.1016/j.isprsjprs.2017.06.013
Zhu, Z., & Woodcock, C. E. (2014). Automated cloud, cloud shadow, and snow detection in multitemporal Landsat data: An algorithm designed specifically for monitoring land cover change. *Remote Sensing of Environment*, *152*, 217-234.https://doi.org/10.1016/j.rse.2014.06.012
Zhu, Z., & Woodcock, C. E. (2014). Continuous change detection and classification of land cover using all available Landsat data. *Remote sensing of Environment*, *144*, 152-171.https://doi.org/10.1016/j.rse.2014.01.011